Parameterization of Cloud Optical Properties for a Mixture of Ice Particles for use in Atmospheric Models

Ming-Dah Chou, Kyu-Tae Lee, Ping Yang

Popular Summary

Submitted to the Journal of Geophysical Research

Cirrus are the most extensive clouds in the tropics. They not only reflect but also absorb strongly the solar radiation due to the large size of ice particles. The impact of cirrus on climate is a long unsettled issue, and it requires reliable radiative transfer calculations to resolve this issue. Based on the detailed high-spectral resolution calculations of cirrus optical properties, the bulk properties of cirrus have been parameterized as a function of the mean size of a mixture of ice particles with various shapes. The fast and accurate parameterization has been implemented into the Goddard radiation scheme for use in cloud and climate models.

Dr. Ming-Dah Chou, Laboratory for Atmospheres, NASA/Goddard Space Flight Center, Greenbelt, MD 20771

Prof. Kyu-Tae Lee, Department of Atmospheric and Environmental Science, National Kangnung University, Kangnung, South Korea

Prof. Ping Yang, Department of Atmospheric Sciences, Texas A&M University, College Station, TX 77843

ABSTRACT

Based on the single-scattering optical properties that are pre-computed using an improve geometric optics method, the bulk mass absorption coefficient, single-scattering albedo, and asymmetry factor of ice particles have been parameterized as a function of the mean effective particle size of a mixture of ice habits. The parameterization has been applied to compute fluxes for sample clouds with various particle size distributions and assumed mixtures of particle habits. Compared to the parameterization for a single habit of hexagonal column, the solar heating of clouds computed with the parameterization for a mixture of habits is smaller due to a smaller co-single-scattering albedo. Whereas the net downward fluxes at the TOA and surface are larger due to a larger asymmetry factor. The maximum difference in the cloud heating rate is ~ 0.2 $^{\circ}C\ day^{-1}$, which occurs in clouds with an optical thickness > 3 and the solar zenith angle < 45°. Flux difference is < 10 $W\ m^{-2}$ for the optical thickness ranging from 0.6 to 10 and the entire range of the solar zenith angle. The maximum flux difference is ~ 3%, which occurs around an optical thickness of 1 and at high solar zenith angles.

1. Introduction

Cirrus clouds have a large impact on climate for two reasons. The location of these clouds at the top of the troposphere makes them interact radiatively with the space with minimal interference by the atmosphere above, and they are generally believed to be the most extended clouds even though it is difficult to detect the widespread thin cirrus clouds from satellite radiance measurements. The effect of cirrus on the earth radiation budgets and, hence, climate depends on the thickness of these clouds. For optically thick cirrus, the increase in reflection of the solar radiation is larger than the decrease in the thermal infrared radiation, resulting in a net cooling of the Earth. For optically thin cirrus clouds, the reverse is true. Thus, the net effect of these clouds on climate is dependent upon the relative areal coverage of the thin and thick clouds. Although cirrus reflect strongly the solar radiation, they also absorb strongly the solar radiation due to the large size of ice particles [*Chou et al.*, 1998]. The effect of cirrus on the solar heating of the atmosphere is a long unsettled issue [cf. *Chou et al.*, 2001 and the references cited therein]. To resolve these issues, it requires reliable satellite retrievals of cirrus clouds and radiative transfer calculations of solar radiation.

The single-scattering properties, such as the extinction cross-section, single-scattering albedo, and the scattering phase function, of ice particles are functions of the particle morphology (or shape, habit) and sizes. In situ observations based on airborne two-dimensional cloud probe or balloon-borne replicator have shown that cirrus clouds are almost exclusively composed of nonspherical ice crystals including bullet rosettes, hallow columns, and aggregates [e.g., *Heymsfield and Platt*, 1984; *Arnott et al.* 1994]. Various accurate and approximate methods have been developed to solve the problem of light scattering by nonspherical particles, which have been reviewed by *Mishchenko et al.* [1999]. In particular, the finite-difference time domain or the discrete dipole approximation can be used for size parameters less than 20, and the geometric optics method can be applied to larger particles. Using an improved version of the geometric optics method developed by *Yang and Liou* [1996], *Yang et al.* [2000] computed the single-scattering properties for individual ice crystals with various habits and sizes at wavelengths covering 0.2-5 μm. It produces very useful basic data sets for computing solar heating of a cirrus-laden atmosphere.

For application to weather and climate studies, *Fu* [1996] and *Chou et al.* [1998] developed parameterizations for the bulk single-scattering properties of cirrus clouds assuming a single habit of hexagonal ice particles. Based on *Yang's et al.* [2000] extensive data sets of the single-

scattering properties, *Key et al.* [2002] developed parameterizations for the single-scattering properties individually for seven ice habits. While these parameterizations are very useful, it is not clear how well they can be applied to clouds with a mixture of particle habits. The purpose of this study is to develop parameterizations for the bulk single-scattering properties of clouds with a mixture of particle habits.

2. Single-scattering properties and sample clouds

Using the improved geometric optics method developed by *Yang and Liou* [1996], *Yang et al.* [2000] calculated the extinction efficiency, the scattering efficiency, and the asymmetry factor of individual ice particles. The computed optical properties cover 56 wavelength bands in the range 0.2-5.0 μm, six habits (plates, solid columns, hollow columns, planar bullet rosettes, spatial bullet rosettes, aggregates), and 24 size bins. For a given habit, the ratio of the length to width (aspect ratio) is specified as a function of length based on various *in situ* observations with results reported in several papers [*Auer and Veal*, 1970; *Arnott et al*, 1994; *Greenler*, 1980; *Mitchell and Arnott*, 1994; *Pruppachar and Klett*, 1980]. Hence, the size of a particle is uniquely defined by its length. We use the three-dimensional (habit, size, wavelength) tables of the single-scattering properties pre-computed by *Yang et al.* [2000] to parameterize the bulk optical properties of ice clouds.

A total of 30 sample clouds are used in this study. Each sample cloud is represented by a particle size distribution $n(L)$, where L is the maximum length of a particle. Among the 30 samples, twenty-eight are the same as that used by *Fu* [1996], and two are taken from *Mitchell and Arnott* [1994]. Twenty-one samples are mid-latitude clouds, and nine samples are equatorial clouds. These clouds were also used by *Key et al.* [2002] to parameterize optical properties of individual ice habits.

For a given particle size, L, the percentage of an ice crystal habit is specified for mid-latitude clouds and equatorial clouds. For mid-latitude cirrus clouds, the percentage information is derived from the statistics based on FIRE-I and II data, and is given as follows:

50% bullet rosettes, 25 % plates, 25% hollow columns for L<70μm

30% aggregates, 30% bullet rosettes, 20% hollow columns for L>70 μm.

Note that this percentage model has been used for cirrus microphysical model involved in the forward radiative transfer calculations for generating look-up libraries used in the Moderate-Resolution Imaging Spectroradiometer (MODIS) Airborne Simulator (MAS) cirrus retrieval

algorithm [*Baum et al.*, 2000]. For tropical cirrus cloud system, the habit percentage is derived from CEPEX data [*McFarquhar*, 2000] and is given by:

33.7% columns, 24.7% bullet rosettes, 41.6% aggregates for all L.

With the pre-computed single-scattering properties and the sample clouds defined above, the mean extinction cross section, or volume extinction coefficient, σ at wavelength λ for a mixture of habits is computed from

$$\sigma(\lambda) = \int \left[\sum_i Q_{e,i}(L,\lambda) A_i(L) f_i(L) \right] n(L) dL \tag{1}$$

where the subscript i denotes the habit, $Q_{e,i}$ is the pre-computed extinction efficiency, and A_i is the projected area of a particle perpendicular to the light when randomly oriented in space. The mean extinction efficiency can then be defined as

$$Q_e(\lambda) = \frac{\sigma(\lambda)}{A} \tag{2}$$

where A is the total projected area of the particles given by

$$A = \int \left[\sum_i A_i(L) f_i(L) \right] n(L) dL \tag{3}$$

It has been demonstrated in a number of investigations [e.g. *Hansen and Travis*, 1974; *Foot*, 1988; *Wyser and Yang*, 1998] that the bulk optical properties of both liquid and ice clouds can be well defined by the effective particle size that is proportional to the ratio of the total volume to the total projected area of particles. The detailed distributions of particle size are not essential. According to Francis et al. [1994], we define the effective particle size of a cloud layer with a mixture of various habits and sizes as

$$D_e = \frac{3}{2}\frac{V}{A} = \frac{3}{2}\frac{C}{\rho_{ice} A} \tag{4}$$

where C is the concentration of ice particles in mass per unit volumn, ρ_{ice} = 0.9167 g cm^{-3} is the density of ice, and V is the total volume of ice particles given by

$$V = \int \left[\sum_i V_i(L) f_i(L) \right] n(L) dL \tag{5}$$

From Equations (2) and (4), the extinction cross section becomes

$$\sigma(\lambda) = \frac{3}{2}\frac{Q_e(\lambda)}{\rho_{ice} D_e} C \tag{6}$$

and the optical thickness τ of a layer with a geometric thickness Δz is given by

$$\tau(\lambda) = \beta(\lambda) IWP \tag{7}$$

where

$$\beta(\lambda) = \frac{3}{2}\frac{Q_e(\lambda)}{\rho_{ice} D_e} \tag{8}$$

is the mass extinction coefficient, and $IWP = C\Delta z$ is the ice water content of a layer. It is noted that ice particles are large, and $Q_e \sim 2$. From Equation (8), we have

$$\beta(\lambda) \approx \frac{3.273}{D_e} \tag{9}$$

where the unit is $m^2\ g^{-1}$ for β and μm for D_e. Finally, the mean single-scattering albedo ω and asymmetry factor g of ice clouds are computed from

$$\omega(\lambda) = \frac{\int \left[\sum_i Q_{s,i}(L,\lambda) A_i(L) f_i(L) \right] n(L) dL}{\int \left[\sum_i Q_{e,i}(L,\lambda) A_i(L) f_i(L) \right] n(L) dL} \tag{10}$$

$$g(\lambda) = \frac{\int \left[\sum_i g_i(L,\lambda) Q_{s,i}(L,\lambda) A_i(L) f_i(L) \right] n(L) dL}{\int \left[\sum_i Q_{s,i}(L,\lambda) A_i(L) f_i(L) \right] n(L) dL} \tag{11}$$

where $Q_{s,i}$ is the scattering efficiency, and g_i is the asymmetry factor, both are pre-computed as functions of habitat, size, and wavelength.

3. Parameterization for bulk cloud single-scattering properties

Because of the constraint on computing time, the solar spectrum is divided into a limited number of bands in our solar radiation parameterization [*Chou et al*, 1998, 1999]. In the ultra-

violet (UV) and visible spectral region ($\lambda < 0.7\ \mu m$), the absorption due to O_3 and the Rayleigh scattering due to gases vary smoothly with wavelength. The spectral range from 0.175 to 0.7 μm is divided into 8 narrow bands. A mean O_3 absorption coefficient and a mean Rayleigh scattering extinction coefficient are assigned for each of the eight bands. In the infrared spectral region from 0.7 to 10 μm, the absorption due to water vapor varies rapidly with wavelength. This region is divided into three wide bands, similar to that of *Slingo* [1989] except it is extended to 10 μm in the thermal infrared. Each of these three bands is arranged into 10 intervals of the absorption coefficient k, and the k-distribution method is applied to compute fluxes. The spectral ranges of the 11 bands are given in Table 1.

The mean mass extinction coefficient, β, co-single-scattering albedo, $1\text{-}\omega$, and asymmetry factor, g, of the 11 spectral bands are parameterized as functions of the effective particle size, D_e. For each of the 30 sample clouds, a value of D_e is computed from Equations (3)-(5). As in *Chou et al.* [1998], the mean extinction coefficient is derived from,

$$\beta = \sum \beta_\lambda S_\lambda \Delta\lambda \,/\, \sum S_\lambda \Delta\lambda \tag{12}$$

where S is the solar insolation at the top of the atmosphere (TOA) and $\Delta\lambda$ is the spectral interval of the 56 wavelength bands at which the single-scattering properties are pre-computed. The summations are applied to the spectral bands. It is noted that the precomputed single-scattering properties cover the spectral region from 0.2 to 5.0 μm, [*Yang et al.*, 2000] but the spectral range of Band 11 in our shortwave radiation scheme extends to 10 μm in the thermal infrared (see Table 1). The effect of the extinction coefficient in 5.0-10.0 μm is not taken into consideration in computing the mean extinction coefficient of Band 11 from Equation (12), Since the insolation S in this spectral region is small, the effect on β is also small.

The co-single-scattering albedo varies greatly within a spectral band (see Figure 1 of *Chou et al.*, 1998). Thus, the form for averaging $(1\text{-}\omega_\lambda)$ over a wide spectral band such as those shown in Table 1 should vary with the strength of absorption. The averaging should be linear for weak absorption and logarithmic for strong absorption. Following *Chou et al.* [1998], it is derived from

$$(1-\omega) = h(1-\omega') + (1-h)(1-\omega'') \tag{13}$$

where

$$(1-\omega') = \sum (1-\omega_\lambda)\beta_\lambda S_\lambda \Delta\lambda / \sum \beta_\lambda S_\lambda \Delta\lambda \tag{14}$$

$$\ln(1-\omega'') = \sum \ln(1-\omega_\lambda)\beta_\lambda S_\lambda \Delta\lambda / \sum \beta_\lambda S_\lambda \Delta\lambda \tag{15}$$

and h is the weight which varies with the strength of absorption. It is empirically chosen to be 1 for Bands 1-8, 2/3 for Band 9, 1/3 for Band 10, and 0 for Band 11. Finally, the mean asymmetry factor is derived from

$$g = \sum g_\lambda \omega_\lambda \beta_\lambda S_\lambda \Delta\lambda / \sum \omega_\lambda \beta_\lambda S_\lambda \Delta\lambda \tag{16}$$

With β, ω, and g computed for each of the 11 spectral bands and the 30 sample clouds, which correspond to 30 values of D_e, they are parameterized according to

$$\beta = a_0 / D_e \tag{17}$$

$$1-\omega = b_0 + b_1 D_e + b_2 D_e^2 \tag{18}$$

$$g = c_0 + c_1 D_e + c_2 D_e^2 \tag{19}$$

where a, b, and c are regression coefficients.

Figure 1 shows the extinction coefficient as a function of the effective particle size. The extinction coefficient for all bands fall onto a single curve given by (17) with a_0=3.276 $m^2\ g^{-2}\ \mu m$, which is nearly identical with that of Equation (9). It is noted that the definition of the effective particle size used in *Chou et al.* [1998] follows that of *Fu* [1996], which is different from that of Equation (4) and is given by

$$D_{ge} = \frac{2\sqrt{3}}{3}\frac{C}{\rho_{ice} A} \tag{20}$$

From Equation (4), we have

$$D_{ge} = 0.7698\ D_e \tag{21}$$

The difference in the definitions of the effective particle size has been taken into account for the comparison shown in Figure 1.

The coefficients b and c are shown in Table 2 for Bands 6-11. For Bands 1-5, the solar radiation is nearly totally absorbed in the stratosphere, and clouds have little effect on the solar heating of the atmosphere and the surface. Parameterizations for cloud optical properties in these bands are irrelevant to flux calculations. The regression of Equation (18) for a mixture of particle habits is shown by the curves in Figure 2 for Bands 9-11. For Bands 1-8, the co-single-scattering albedo is $< 10^{-5}$, and the results are not shown. The dots in the figure are the co-single-scattering albedo of the 30 sample clouds computed from the parameterization of *Chou et al.* [1998], which assumed that the habit of all cloud particles is hexagonal solid column. The difference is small between the particles with a single habit of hexagonal and that with a mixture of habits, except for Band 11 and $D_e < 20\ \mu m$. The extinction and absorption efficiencies are mainly dependent on the ratio of particle volume to projected area, a parameter that approximately corresponds to the mean path length of photons within the particle in the process of photon phase delay and absorption [*Bryant and Latimer*, 1969]. For a given ratio of the particle volume to the projected area (i.e., the effective size defined in this study), the effect of particle morphology is significant at resonant region where the dimension of the wavelength of radiation is comparable to the size of particles. In addition, the effect of particle geometry on absorption is more significant when absorption is stronger. For bands 1-9, the sizes of small ice crystals are substantially larger than incident wavelengths at which absorption is weak. On the contrary, many particles in the particle population have size parameters in resonant region when D_e is smaller than 20 μm.

Figures 3 shows the regression curves of Equation (19) that fit the mean asymmetry factor g for the 30 sample clouds. The magnitude of g is within the range from 0.74 to 0.91 and increases with increasing particle size and wavelength. The dots represent the parameterization of *Chou et al.* [1998] assuming all particles are hexagonal. It is noted that *Chou et al.* [1998] parameterized the asymmetry factor for the entire UV and visible region and only one set of g is given for this region. The maximum difference in g between a mixture of habits and a single habit of hexagonal particles is ~0.03.

4. Impact of parameterization on flux and heating rate calculations

Although it is generally acknowledged that absorption and reflection of solar radiation by clouds depends strongly on the effective particle size and that the detailed distribution of particle size is not important, it is not clear whether the shape of cloud particles has a significant impact on solar radiation. The results shown in Figures. 1-3 indicate that the shape of cloud particles has no effect on the optical thickness and only a moderate effect on the single scattering albedo and

asymmetry factor. To provide information on the effect of cloud particle habit on the solar heating of the atmosphere and the surface, we implement in the solar radiation model of *Chou et al.* [1999] two sets of parameterizations for cloud optical properties. One is the parameterization of the present study, which takes into account the mixture of particle habits, and the other is that of *Chou et al.* [1998], which assumes only a single hexagonal habit.

A homogeneous cloud is assumed to be in the layer 325-396 *hPa* with an ice water content (*IWP*) of 30 $g\ m^{-2}$. The profiles of temperature, humidity, and ozone typical of a mid-latitude summer are used. The atmosphere is divided into 59 layers. There are three layers spanning the cloud with a constant thickness of 23.8 *hPa* for each layer. The surface albedo is assumed to be 0.2 for all spectral bands. Fluxes are computed for the 30 sample clouds mentioned in Section 2. One value of D_e is computed for each of the 30 sample clouds using Equation (4) with A and V given by Equations (3) and (5). The optical thickness, single-scattering albedo, and asymmetry factor are then computed from Equations (7) and (17)-(19) for individual spectral bands. As can be seen from Equations (7) and (17) that, for *IWP*= 30 $g\ m^{-2}$, the optical thickness is uniquely related to D_e by

$$\tau = \frac{98.3}{D_e} \tag{22}$$

where the unit of D_e is μm. Values of D_e for the 30 sample clouds can be identified by the dots given in Figures 1-3, and 7-8.

The impact of the parameterization based on a mixture of habits and a single habit of hexagonal solid column is shown in Figure 4 for the flux at TOA (left panels) and the surface (right panels). The upper panels show the absolute flux difference in $W\ m^{-2}$, and the lower panels show the difference in 0.1% relative to the fluxes computed using the present parameterization. The difference refers to the results of the present parameterization based on a mixture of habits minus that based on a single habit of hexagonal particles. It can be seen that the maximum difference is ~ 3% at D_e ~ 80 μm (or τ ~1) and high solar zenith angles. The difference is positive due to a larger g for a mixture of habits than that for the hexagonal particles, as shown in Figure 3. The positive difference is slightly larger at the surface than at TOA due to a weaker absorption of clouds with mixed habits than that with hexagonal ice particles, especially in Band 11 as shown in Figure 2. Figure 5 shows the difference between two sets of identical flux calculations except the asymmetry factor g is computed differently; one from the present parameterization for a mixture of habits, and the other from that of *Chou et al.* [1996] for a single habit of hexagonal

particles. By comparing Figure 5 with Figure 4, it can be seen that over 85% of the difference shown in Figure 4 are due to the difference in the asymmetry factor.

Figure 6 shows the difference in the absorption of solar radiation by the clouds due to the different parameterizations for the cloud optical properties. The left panel is the difference in solar heating in $W\ m^{-2}$, and the right panel is the percentage difference. The difference is negative indicating that the solar heating of the cloud layer is weaker when parameterization is based on a mixture of cloud habits than that based on hexagonal ice particles. For the cloud thickness of 71 hPa, a difference of 1 $W\ m^{-2}$ in the absorption of solar radiation is equivalent to a heating rate difference of ~0.12 $^{\circ}C\ day^{-1}$. The left panel of the figure shows that the effect of the cloud habit on the heating of the cloud layer is generally less than 1 $W\ m^{-2}$, or ~0.12 $^{\circ}C\ day^{-1}$, except for a small solar zenith angle and a small D_e (or equivalently a large optical thickness).

Information on the size distribution of cloud particles is adequate for computing the effective particle size for the spherical particles of water clouds but not for the non-spherical particles of ice clouds. Figure 7 shows the effective size of the ice particles for the 30 sample clouds when assuming different cloud habits. It is computed from Equations (3)-(5). Only the effective particle size of three habits (bullet rosettes, solid columns, aggregates) and a mixture of habits used in the parameterization (see Section 2) are shown. Among these habits of ice particles, the effective particle size is the largest for aggregates and smallest for rosettes. The effective particle size is primarily determined by the assigned aspect ratio, which varies with the habit and length of ice particles. The figure shows that the effective particle size could vary by a factor of two due to different particle habits. The effect of habits on the flux calculations at TOA for a solar zenith angle of 30° is shown in Figure 8. The difference in habits could induce an error greater than 100 $W\ m^{-2}$ in the TOA flux for clouds with a small D_e, which is equivalent to a large τ for a fixed IWP.

5. Conclusions

Using the improved geometric optics method, *Yang et al.* [2000] computed the single-scattering optical properties of individual ice particles as a function of particle habit, particle size, and wavelength. Based on these pre-computed single-scattering optical properties, we have computed the mean effective particle size, mass absorption coefficient, single-scattering albedo, and asymmetry factor for 30 sample cirrus clouds. Each sample cloud is identified with a particle size distribution, a composition of particle habits, and the aspect ratios of particle size dimension. We then develop parameterizations for the bulk mass absorption coefficient, single-scattering

albedo, and asymmetry factor as a function of the mean effective particle size. Thus, our parameterization applies to ice clouds with a mixture of particle habits. The parameterization differs from that of *Fu* [1996] and *Chou et al.* [1998] that considered only the hexagonal particles. It also differs from that of *Key et al.* [2002] that separately parameterized the optical properties for individual particle habits.

The parameterizations have been applied to compute fluxes for the 30 sample clouds and the entire range of the solar zenith angle. The effective particle size of these sample clouds ranges from 10 to 150 μm. By specifying the cloud ice water content at 30 $g\ m^{-2}$, the optical thickness of these clouds ranges from 0.6 to 10. Compared to the parameterization of [*Chou et al.*, 1998] for hexagonal ice particles, the solar heating of clouds computed with the parameterization for a mixture of particle habits is smaller due to a smaller co-single-scattering albedo, whereas the net downward fluxes at the TOA and surface are larger due to a larger asymmetry factor. The maximum difference in the cloud heating rate is ~ 0.2 $^{\circ}C\ day^{-1}$, which occurs in clouds with an optical thickness > 3 and the solar zenith angle < 45°. Flux difference is < 10 $W\ m^{-2}$ for the optical thickness ranging from 0.6 to 10 and the entire range of the solar zenith angle. The maximum flux difference is ~ 3%, which occurs around an optical thickness of 1 and at high solar zenith angles.

For a given size distribution of ice particles, the effective size varies significantly with particle habit due to different shapes and aspect ratios of particle dimension. Consequently, the optical thickness and, hence, fluxes vary significantly with particle habits. Model calculations show that the net downward flux at the top of the atmosphere could differ by as much as 150 $W\ m^{-2}$ for a solar zenith angle of 30° when different particle habits are assumed. It follows that the information on the particle size distribution alone is not sufficient for estimating the effective particle size. The information on particle habit and aspect ratio is also needed for estimating the effective particle size. However, the information on habit and size is generally not available. To overcome this difficulty, *McFarquhar* [2000] developed a parameterization for the effective size as a function of cloud ice water concentration and temperature based on *in situ* observations of the ice water concentration and the total projected cross section of particles. The parameterization can be applied to the atmospheric models where the ice water content is a prognostic parameter. We have implemented *McFarquhar*'s parameterization for the effective particle size together with the parameterizations of this study for the bulk single-scattering properties in our solar radiation scheme for weather and climate studies [*Chou et al.* 1999].

Acknowledgments. The work of M.-D. Chou was supported by the Global Analysis and Modeling Program, NASA/Office of Earth Science. The effort of P. Yang was supported by NASA Radiation Sciences Program.

References

Arnott, W. P., Y. Dong, J. Hallett, and J. Poellot, Role of small ice crystals in radiative properties of cirrus: a case study, FIRE II. November 22, 1991. *J. Geophys. Sci.*, *99*, 1371-1382, 1994.

Auer, A. H., Jr., and D. L. Veal, The dimension of ice crystals in natural clouds, *J. Atmos. Sci.*, *27*, 919-926, 1970.

Baum, A.B., D. P. Kratz, P. Yang, S.C. Ou, Y.X. Hu, P. F. Soulen, and S.-C. Tsay, Remote sensing of cloud properties using MODIS airborne simulator imagery during SUCCESS 1. Data and models, *J. Geophys. Res. 105*, 11,767-11,780, 2000:

Bryant, F. D. and P. Latimer, Optical efficiencies of large particles of arbitrary shape and orientation, *J. Colloid Interface Sci.*, *30*, 291-304, 1969.

Chou, M.-D., and M. J. Suarez, A shortwave radiation parameterization for atmospheric studies, *15*, *NASA Tech Memo*-104606. pp40, 1999.

Chou, M.-D., M. J. Suarez, C-H. Ho, M. M.-H. Yan, and K.T. Lee, Parameterizations for cloud overlapping and shortwave single-scattering properties for use in general circulation and cloud ensemble models, *J. Climate*, *11*, 202-214, 1998.

Chou, M.-D., P.-K. Chan, and M. M.-H. Yan, A sea surface radiation data set for climate applications in the tropical western Pacific and South China Sea. *J. Geophy. Res.*, *106*, 7219-7228, 2001.

Foot, J. S., Some observations of the optical properties of clouds. I: Stratocumulus, *Q. J. R. Meteorol. Soc.*, *114*, 129-144, 1988.

Francis, P. N., A. Jones, R. W. Saunders, K. P. Shine, A. Slingo and Z. Sun, An observational and theoretical study of the radiative properties of cirrus: some results from ICE'89. *Q. J. R. Meteorol. Soc.*, *120*, 809-848, 1994.

Fu, Q., An accurate parameterization of the solar radiative properties of cirrus clouds for climate models, *J. Climate*, *9*, 2058-2082, 1996.

Greenler, R. G., *Rainbow, Halos, and Glories*, 195 pp., Cambridge Univ. Press, New York, 1980.

Hansen, J. E., and L. D. Travis, Light scattering in planetary atmospheres, *Space Sci Rev.*, *16*, 527-610, 1974.

Heymsfield, A.J., and C.M.R. Platt, A parameterization of the particle size spectrum of ice clouds in terms of the ambient temperature and ice water content, *J. Atmos. Sci.*, *41*, 846-855. 1984.

Key, J. R., P. Yang, B. A. Baum, and S. L. Nasiri, Parameterization of shoretrwave ice cloud optical properties for various particle habits, *J. Geophy. Res.*, *32*, 2002.

McFarquhar, G.M., Comments on 'Parameterization of effective sizes of cirrus-cloud particles and its verification against observations' by Zhian Sunand Lawrie Rikus (October B, 1999, 125, 3037-3055), *Quart. J. Roy. Meteor. Soc.*, *126*, 261-266, 2000.

Mitchell, D. L., and W. P. Arnott, A model predicting the evolution of ice particle size spectra and radiative properties of cirrus clouds. II. Dependence of absorption and extinction on ice crystal morphology, *J. Atmos. Sci.*, *51*, 817-832, 1994.

Mishchenko, M.I., W. J. Wiscombe, J.W. Hovenier, and L. D. Larry, Overview of scattering by nonspherical particles, in "Light Scattering by Nonspherical Particles: Theory, Measurements, and Applications", eds. M. I. Mishchenko, J. W. Hovenier, and L.D. Travis, *Academic Press*, San Diego, Californai. 1999.

Pruppacher, H. P. and J. D. Klett, *Microphysics of Clouds and Precipitation*, 714 pp., D. Reidel, Norwell Mass., 1980.

Slingo, A., A GCM parameterization for the shortwave radiative properties of water clouds, *J. Atmos. Sci.*, *46*, 1419-1427, 1989.

Wyser, K., and P. Yang, Average ice crystal size and bulk shortwave single-scattering properties of cirrus clouds, *Atmos. Res.*, *49*, 315-335, 1998.

Yang, P., and K.-N. Liou, Geometric-optics-integral-equation method for light scattering by nonspherical ice crystals, *Appl. Opt.*, *35*, 6568-6584, 1996.

Yang, P., and K.-N. Liou, K. Wyser, and D. Mitchell, Parameterization of the scattering and absorption properties of individual ice crystals, *J. Geophy. Res.*, *105*, 4699-4718, 2000.

Table 1. Spectral ranges of the solar radiation scheme.

Band	Spectral Range (μm)
1	0.175-0.225
2	0.225-0.245; 0.260-0.280
3	0.245-0.260
4	0.280-0.295
5	0.295-0.310
6	0.310-0.320
7	0.320-0.400
8	0.400-0.700
9	0.700-1.220
10	1.220-2.270
11	2.270-10.00

Table 2. Coefficients for the parameterizations for ω and g using Eqs. (18) and (19).

Band	b_o	b_1	b_2	c_o	c_1	c_2
5	1.33e-07	8.12e-08	3.36e-12	7.55e-01	1.09e-03	-4.13e-06
6	1.37e-07	7.06e-08	5.64e-12	7.56e-01	1.08e-03	-4.12e-06
7	1.37e-07	7.06e-08	5.64e-12	7.56e-01	1.08e-03	-4.12e-06
8	-1.52e-07	7.38e-08	-3.48e-11	7.46e-01	1.41e-03	-5.74e-06
9	1.41e-06	5.72e-06	-1.22e-09	7.25e-01	1.85e-03	-7.73e-06
10	1.12e-03	5.65e-04	-8.96e-07	7.17e-01	2.28e-03	-8.86e-06
11	4.83e-02	2.74e-03	-9.02e-06	7.71e-01	2.45e-03	-1.00e-05

Figure Captions

Figure 1. The extinction coefficient as a function of the effective particle size. The curve is the parameterization of this study for a mixture of ice particle habits, and the dots are taken from *Chou et al.* [1998] for a single habit of hexagonal particles. The parameterizations apply to all solar spectral bands.

Figure 2. Same as Figure 1, except for the co-single-scattering albedo and for Bands 9-11 shown in Table 1.

Figures 3. Same as Figure 2, except for the asymmetry factor and for Bands 6-11.

Figure 4. Impact of different parameterizations for cloud optical properties on the flux calculations (mixture of habits minus solid column) at the top of the atmosphere (TOA) and at the surface. The upper panels show the absolute flux difference in $W\,m^{-2}$, and the lower panels show the relative difference in 0.1%.

Figure 5. Same as Figure 4, except that the impact is only due to different parameterizations for g.

Figure 6. Impact of different parameterizations for cloud optical properties on the solar heating of the cloud layer (mixture of habits minus solid column). The left panel is the difference in solar heating in $W\,m^{-2}$, and the right panel is the percentage difference relative to the cloud heating.

Figure 7. The effective particle size of the 30 sample clouds when assuming different ice particle habits.

Figure 8. The effect of particle habits on flux calculations at TOA for a solar zenith angle of 30°.

Figure 1

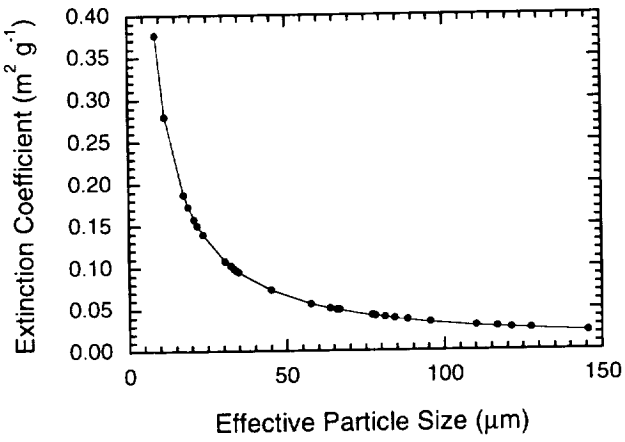

Figure 2

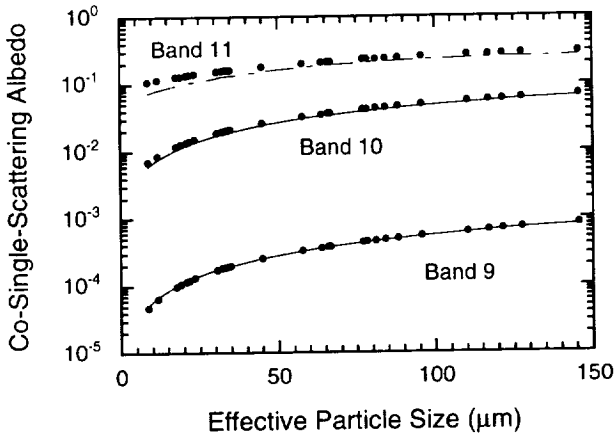

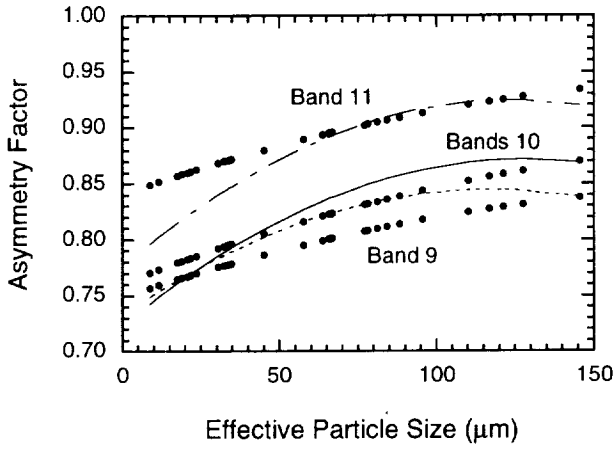
1.00
0.95
0.90
0.85
0.80
0.75
0.70
Asymmetry Factor
Band 11
Bands 10
Band 9
0
50
100
150
Effective Particle Size (μm)

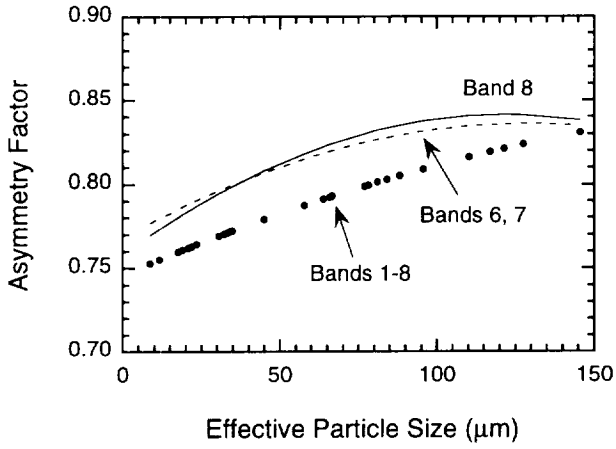
0.90
0.85
0.80
0.75
0.70
Asymmetry Factor
Band 8
Bands 6, 7
Bands 1-8
0
50
100
150
Effective Particle Size (μm)

Figure 3

Figure 1

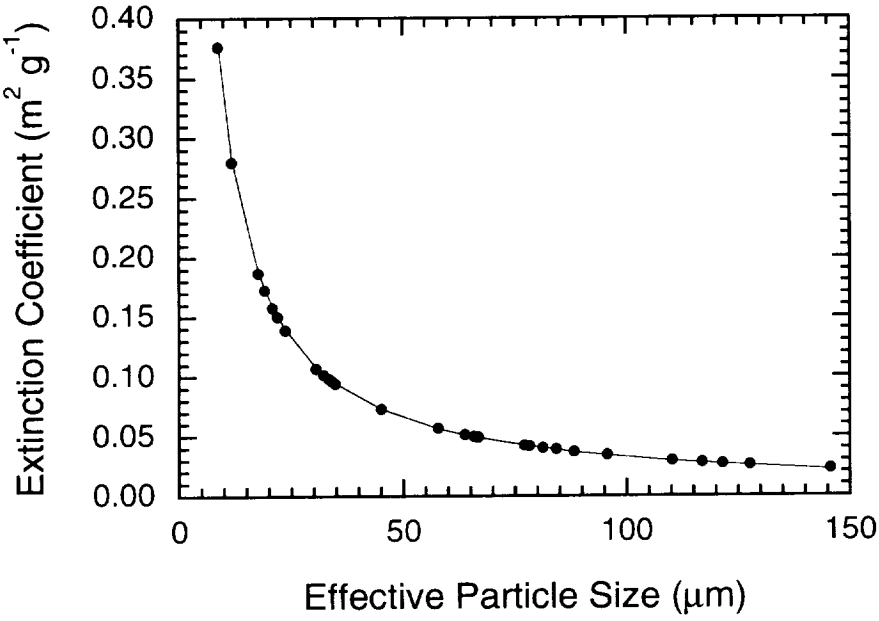
Extinction Coefficient ($m^2 g^{-1}$)
0.40
0.35
0.30
0.25
0.20
0.15
0.10
0.05
0.00
0
50
100
150
Effective Particle Size (μm)

Figure 2

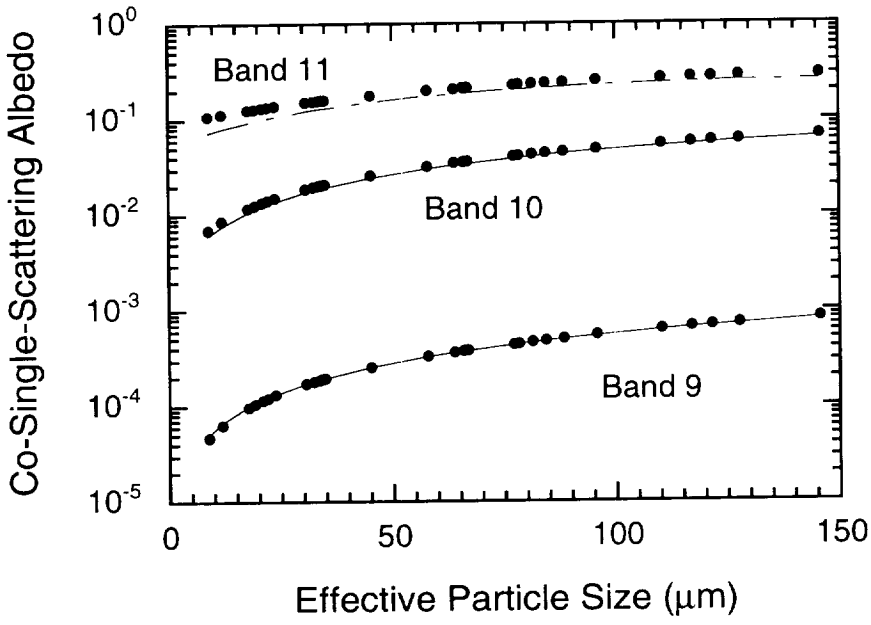
Co-Single-Scattering Albedo
10^0
10^{-1}
10^{-2}
10^{-3}
10^{-4}
10^{-5}
Band 11
Band 10
Band 9
0
50
100
150
Effective Particle Size (μm)

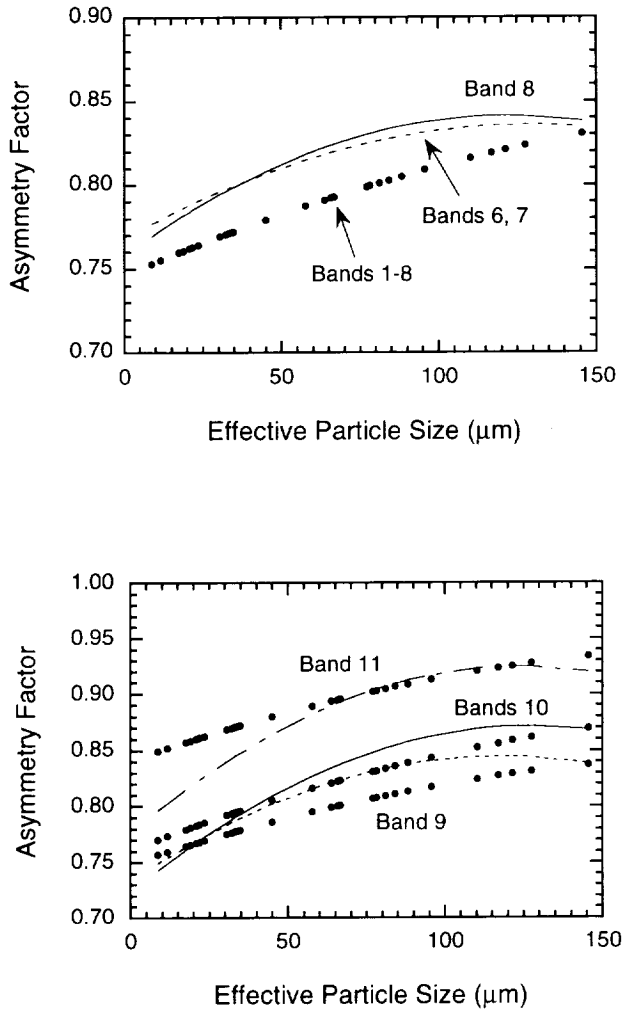
0.90
0.85
0.80
0.75
0.70
Asymmetry Factor
Band 8
Bands 6, 7
Bands 1-8
0
50
100
150
Effective Particle Size (μm)
1.00
0.95
0.90
0.85
0.80
0.75
0.70
Asymmetry Factor
Band 11
Bands 10
Band 9
0
50
100
150
Effective Particle Size (μm)

Figure 3

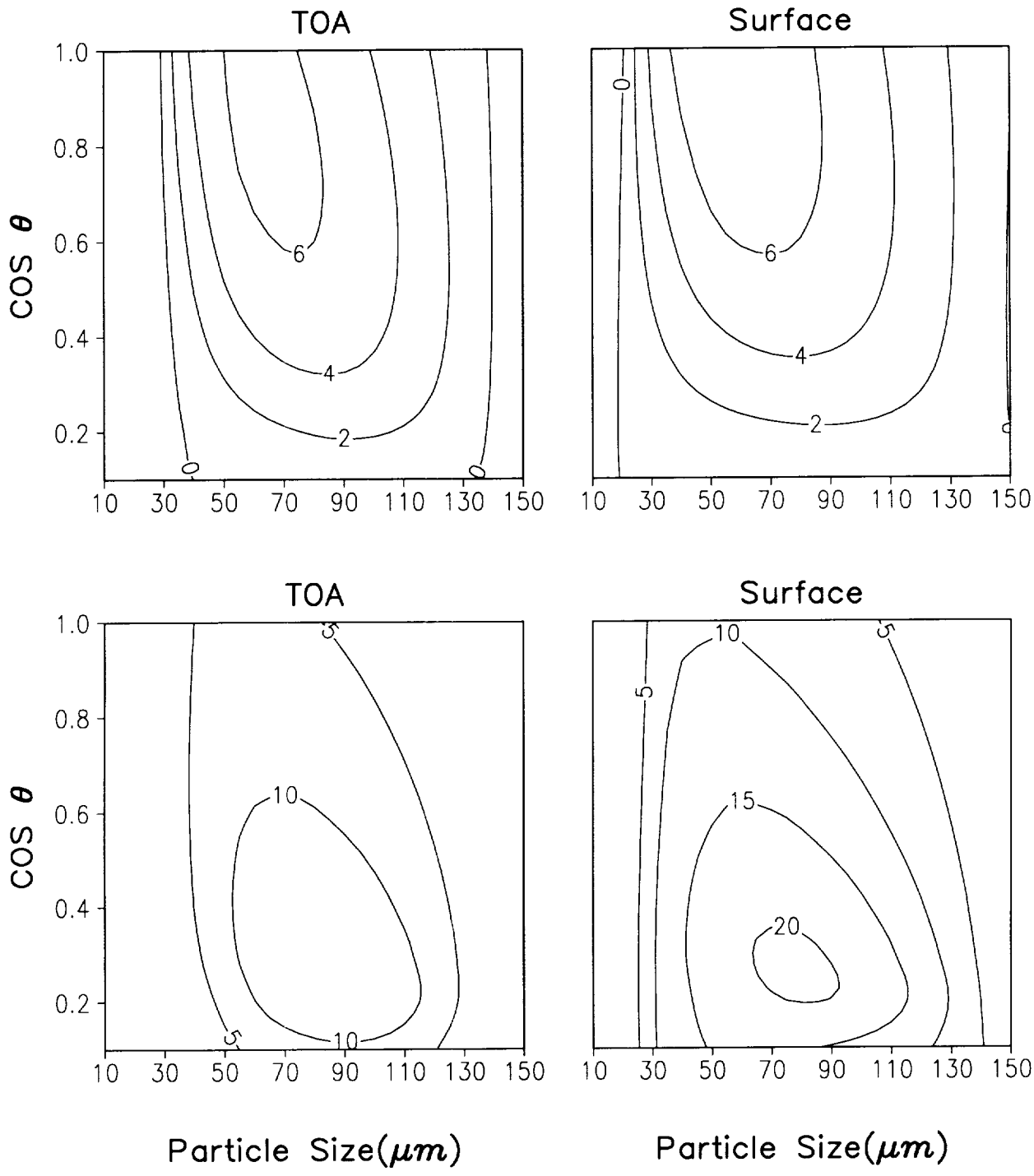
TOA
Surface
TOA
Surface
COS θ
COS θ
1.0
0.8
0.6
0.4
0.2
10 30 50 70 90 110 130 150
0
2
4
6
5
10
15
20
Particle Size(μm)
Particle Size(μm)

Fig.4

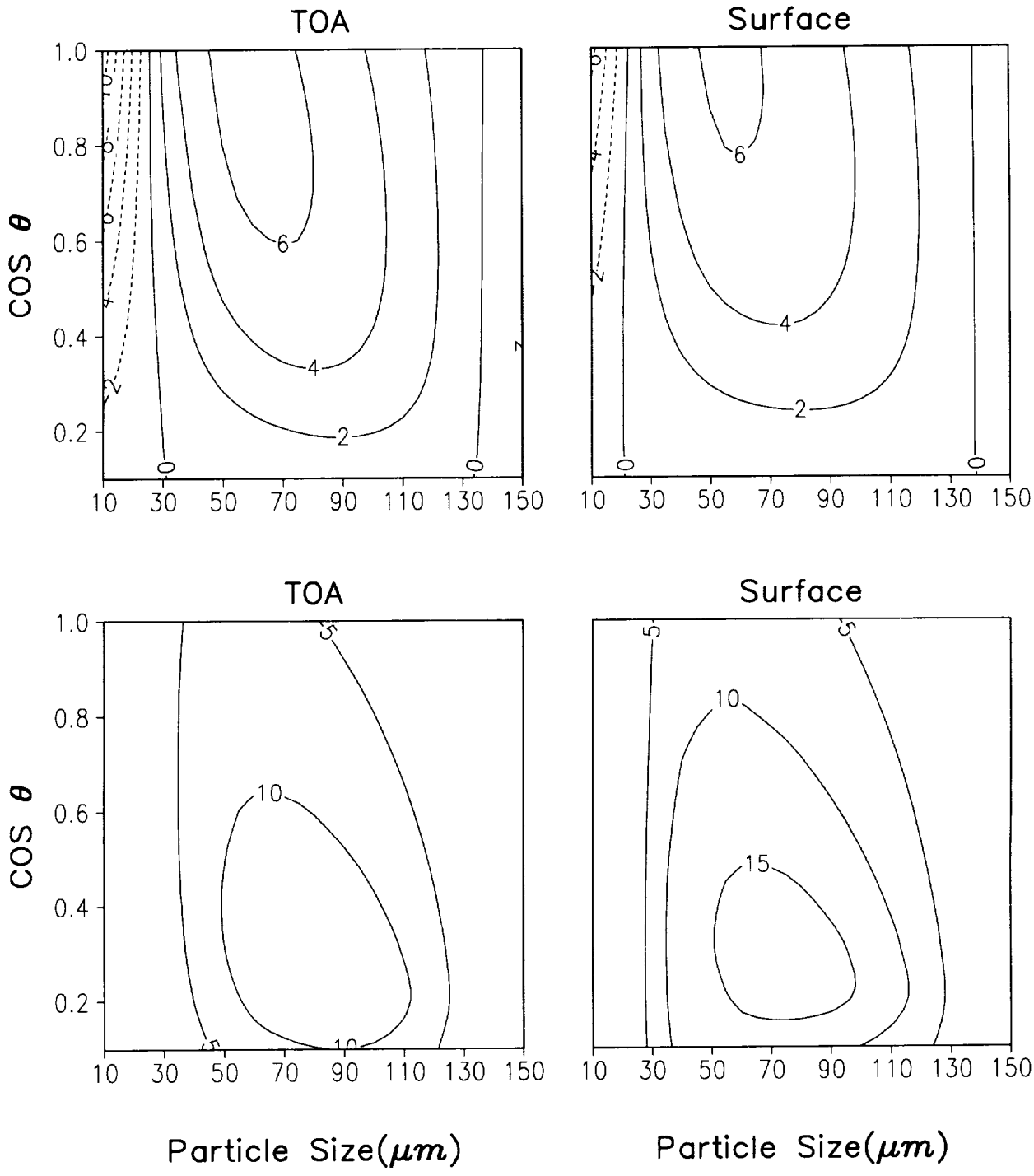
TOA
Surface
TOA
Surface
COS θ
COS θ
1.0
0.8
0.6
0.4
0.2
10 30 50 70 90 110 130 150
Particle Size(μm)
Particle Size(μm)

Fig.5

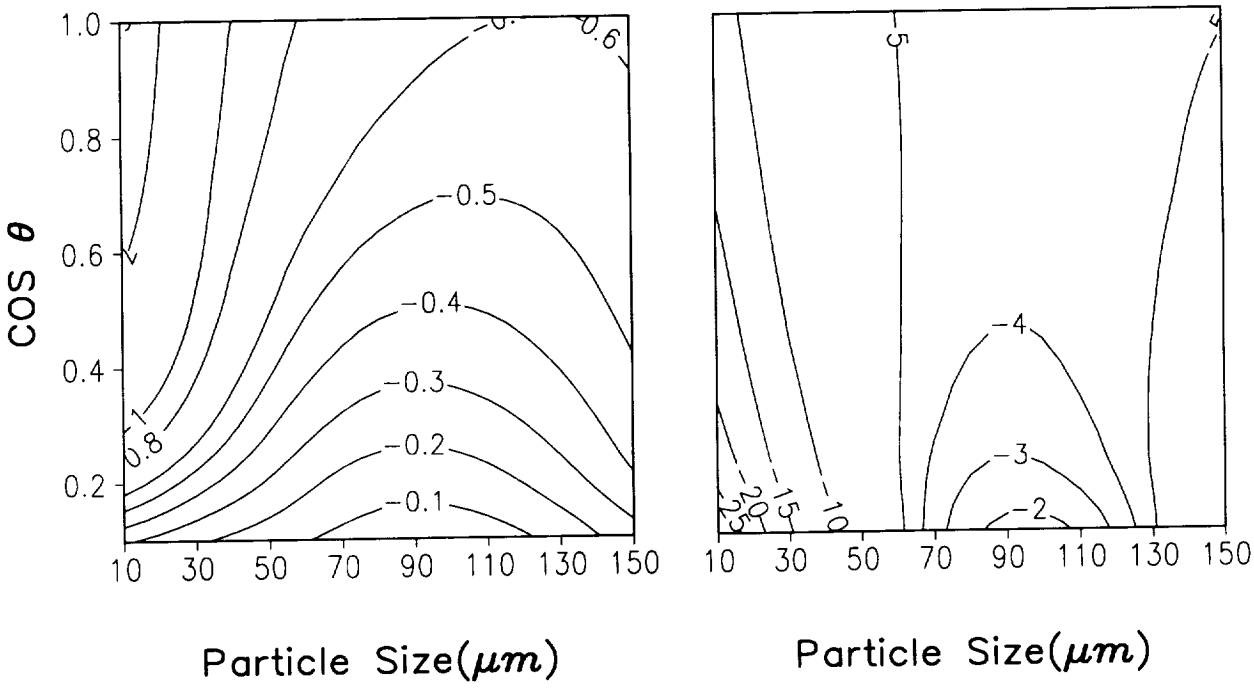
COS θ
1.0
0.8
0.6
0.4
0.2
0.6
0.8
−0.5
−0.4
−0.3
−0.2
−0.1
10 30 50 70 90 110 130 150
Particle Size(μm)
5
−4
−3
−2
10
15
20
25
10 30 50 70 90 110 130 150
Particle Size(μm)

Fig.6

Figure 7

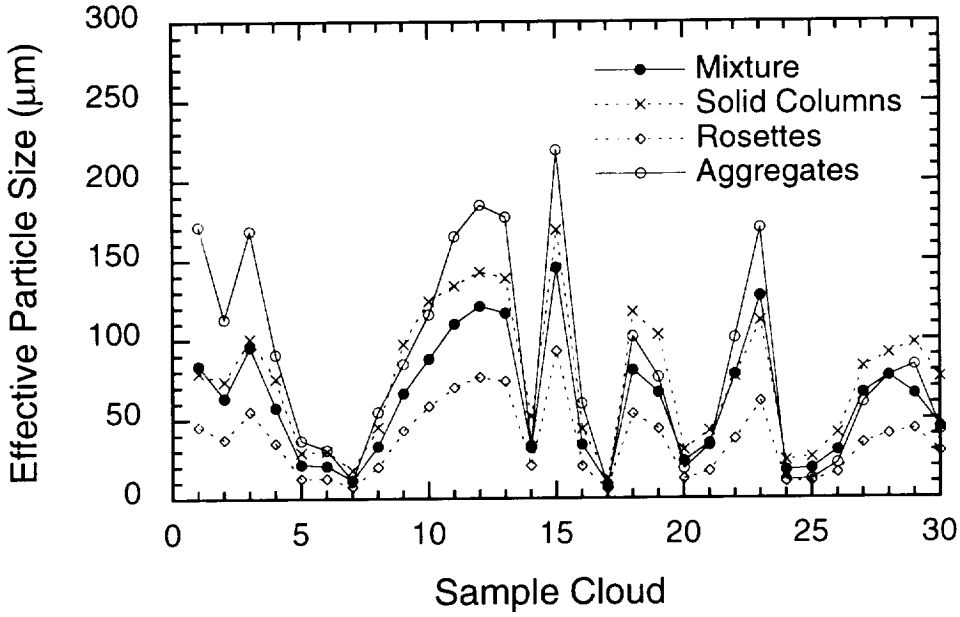
Effective Particle Size (μm)
300
250
200
150
100
50
0
0
5
10
15
20
25
30
Sample Cloud
Mixture
Solid Columns
Rosettes
Aggregates

Figure 8

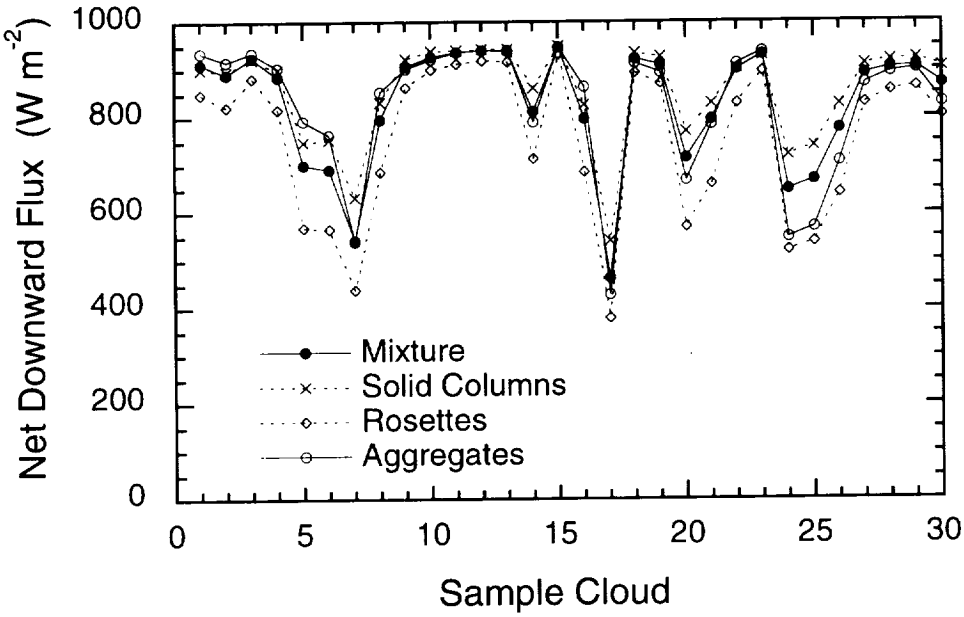
Net Downward Flux (W m-2)
1000
800
600
400
200
0
0
5
10
15
20
25
30
Sample Cloud
Mixture
Solid Columns
Rosettes
Aggregates

Figure 7

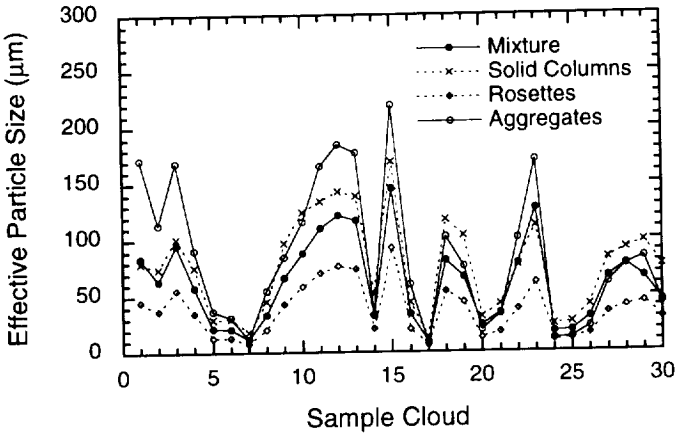

Figure 8